RSC Advances

ROYAL SOCIETY OF CHEMISTRY

www.rsc.org/advances

Ordered Mesoporous Hematite Promoted by Magnesium Selective Leaching as Highly Efficient Heterogeneous Fenton-Like Catalyst

Chunming Zheng[a,*], Xiangzhi Cheng[a], Peipei Chen[a], Chuanwu Yang[a], Shoumin Bao[a], Jun Xia[a], Minglin Guo[a], Xiaohong Sun[b,*]

[a] *State Key Laboratory of Hollow-fiber Membrane Materials and Membrane Processes, School of Environmental and Chemical Engineering, Tianjin Polytechnic University, Tianjin 300387, P.R. China.*

[b] *Key Laboratory of Advanced Ceramics and Machining Technology, Ministry of Education, School of Materials Science and Engineering, Tianjin University, Tianjin 300072, P. R. China*

[*] Corresponding author. Tel.: +86 022 83955661; fax: +86 022 83955140.

E-mail address: zhengchunming@tjpu.edu.cn (C.M. Zheng).

[*] Corresponding author. Tel.: +86 022 27406141; fax: +86 022 27406114.

E-mail address: sunxh@tju.edu.cn (X.H. Sun).

Abstract

Ordered mesoporous hematite with an ultrahigh surface area (up to 200 $m^2 \cdot g^{-1}$) was prepared through a hard templating method of Mg and Fe into mesoporous silica KIT-6 (meso-Mg/Fe_2O_3) and used for the high efficient wet peroxide oxidation of methylene blue. The obtained results showed that approximately two thirds of Mg cations were removed in the leaching process, resulting in a highly porous hematite with a significant amount of defects in the structure. The activated mesoporous iron oxide exhibited excellent catalytic activity for the degradation of methylene blue, achieving above 95 % removal of 60 $mg \cdot L^{-1}$ methylene blue after 3 h at the reaction conditions of initial pH, 0.6 $mg \cdot L^{-1}$ catalyst and 2600 $mg \cdot L^{-1}$ H_2O_2 dosage. The apparent rate constant of used meso-Mg/Fe_2O_3 is 1.972 h^{-1}, which is 1.22, 3.02 and 4.53 times than those of meso-Fe_2O_3, con-Mg/Fe_2O_3 and α-Fe_2O_3. With the increase of reusability of meso-Mg/Fe_2O_3 catalyst, both the leaching concentration of Mg and the catalytic activity of the catalyst increased, which is quite different with the catalytic mechanism of composite components in heterogeneous Fenton-like processes, such as Fe-Cu and Fe-Zn composites. The leaching concentrations of iron in the catalysts were found to be low (<5 $mg \cdot L^{-1}$) in consecutive runs. Hence, meso-Mg/Fe_2O_3 catalyst has proved to be an attractive alternative in the treatment of environmental refractory organic pollutants and have a unique and superb catalytic activity in the heterogeneous Fenton-like system.

Keywords: hematite; Mg substitution; ordered metallic oxides; heterogeneous Fenton; leaching defects

Introduction

The conventional Fenton process requires a strong acid condition (pH < 3) to prevent hydrolysis of ferrous and ferric ions and to maintain acceptable conversion rates. Additionally, non-recyclable soluble iron salts also yields large amounts of iron oxide sludge, which is regarded as a secondary pollution and the loss of catalyst.[1, 2] In order to overcome above disadvantages, the heterogeneous Fenton-like catalysts have been investigated widely. In the past decade, several iron-based catalysts coupled with H_2O_2 for the heterogeneous Fenton-like catalysis have been investigated,[3] i.e. iron oxides and hydroxides[4] iron composites mixed with suitable transition metal such as Co, Mn, Cu, Cr, Zn etc.,[5] supported iron catalysts including oxide supported iron catalysts[6] carbon material supported iron catalysts[7-10] Fe exchanged zeolites, iron exchanged resin, industrial solid waste supported Fe catalysts, and mesoporous material supported Fe catalysts.[11] However, the heterogeneous Fenton-like activities of these catalysts were relatively slow if it was operated at high pH values or without external power supplies such as UV, ultrasound or microwave. Moreover, the leaching of active metals (such as Cu, Co and Cr etc.) also leads to the depletion of their catalytic activity and environmental pollution problems. To overcome these drawbacks of heterogeneous Fenton-like systems, the new developed heterogeneous catalysts should be recyclable in a broad pH range (pH = 3.0- 9.0) and stable to avoid serious leaching of active metals in the operation.[12] Therefore, the key problem is how to design developed heterogeneous Fenton-like catalysts, which can effectively generate ·OH by H_2O_2 decomposition with broad usability and high durability.

Recently, various strategies have been proposed to enhance the performance of heterogeneous Fenton-like catalyst,[13] e.g. loading the catalysts on carriers with high surface area to improve their dispersion,[14] reducing the size of catalyst to nano-scales to increase surface energy.[15] Among these methods, mesoporous iron oxides are of particular interest for they combine large internal surface area, nanosized walls, uniform pore size distributions, large pore volume, controllable compositions and surface functionalities.[16] For example, Cornu C et al. found that the loading of Fe to mesoporous SBA-15 could greatly enhance the degradation performance for methylene blue and studied the formation and location of iron species (including Fe^{2+} and Fe^{3+}) in Fe/SBA-15 catalysts.[17] Xia et al. introduced alumina into Fe-Cu bimetallic oxides supported MCM-41 catalyst to obtain high degradation activities for phenol.[18] But these methods still need to be improved to increase the dispersion of metals active sites on the support and overcome the vulnerable leakage problems of these metals.[19, 20] On the other hand, a wide range of iron-based metal composites with highly ordered mesostructures have been successfully synthesized with a hard templating (nanocasting) method. Some of them exhibited unique heterogeneous Fenton-like catalytic properties.[21, 22] Wang et al. prepared the ordered mesoporous copper ferrite (meso-$CuFe_2O_4$) with KIT-6 hard templating method, which can efficiently increase the degradation activity for imidacloprid.[23] Su et al. reported the substitution of Fe^{2+} by Zn^{2+} can remarkably increase the activity of mesoporous Fe_3O_4 nanoparticles.[24] However, the leaching of active metals (Fe, Cu, Zn et al.) from these mesoporous catalysts was also inevitable, which is undoubtedly lead to the reduction

of their catalytic activity in the long term.

As we all know, the leaching of Mg from mesoporous catalysts was unavoidable and even more serious than active metals such as Fe, Cu, Zn.[25] Hu et al. reported that the leaching concentration of Mg from mesoporous CoMg/SBA-15 was much higher than that of Co. Interestingly, the BET surface area and pore volume also increased after Mg selective leaching in this catalyst system.[26] Jiao et al. reported the fabrication of mesoporous Co_3O_4 with Mg substitution, which exhibited high oxygen evolution activities in visible-light-driven water oxidation system. Approximately a third of Mg cations were removed in the leaching process, resulting in a highly porous cobalt oxide with a significant amount of defects in the spinel structure.[27] In this report, the Mg components in iron-based mesoporous structure are not used as the active metals for the heterogeneous Fenton-like catalysts, but implied to facilitate the leaching process of mesoporous α-Fe_2O_3 substituted by Mg ions. During the selective leaching of Mg ions, the porous structure of α-Fe_2O_3 still remained. Meanwhile, the surface area of the catalyst wasalsoincreased in favor of the adsorption of the macromolecules (Scheme shown in Figure 1).[16, 27]

In this study, highly ordered mesoporous magnesium-substituted α-Fe_2O_3 (meso-Mg/Fe_2O_3) was successfully synthesized through the nanocasting strategy and used as heterogeneous Fenton catalyst with broad usability and enhanced durability. In addition, methylene blue (MB) is a typical synthetic cationic dye which is non-biodegradable, extensively used in textile industry and usually chosen as a model contaminant in the relative studies, whose presence in wastewater may cause the risk

of nausea, vomiting and burn of eye.[11] So MB was selected as a model compound to monitor the Fenton catalytic activity of meso-Mg/Fe_2O_3. The purpose of this study was to elucidate the effect of ordered mesoporous structure and the role of magnesium on the catalytic activity of meso-Mg/Fe_2O_3. For comparison, conventional α-Fe_2O_3, ordered α-Fe_2O_3 and conventional Mg-Fe mixed metal oxides were synthesized as reference catalysts. According to the detected ·OH radical and surface reaction revealed by physico-chemical characterizations, the possible activation mechanism of meso-Mg/Fe_2O_3 was proposed. Finally, the stability and reusability of the catalyst was also investigated.

Experimental

1. Materials

All chemicals required to prepare the mesoporous KIT-6 silica and derived Mg substituted Fe_2O_3 catalysts were used as purchased. Tetraethylorthosilicate (TEOS), triblock copolymer Pluronic P123 (M_w=5800, $EO_{20}PO_{70}EO_{20}$) was purchased from Sigma-Aldrich. Ferric nitrate ($Fe(NO_3)_3 \cdot 9H_2O$), magnesium nitrate ($Mg(NO_3)_2 \cdot 6H_2O$), butyl alcohol, hydrochloric acid (HCl), sodium hydroxide (NaOH), *n*-hexane were obtained from Tianjin Guangfu Chemical Reagent Co., Ltd., China. H_2O_2 (30 %, v/v), ethanol, isopropanol and methylene blue (MB) were supplied by Shanghai Aladdin Chemical Reagent Co., Ltd, China. Deionized water was used through out the experiments.

2. Synthesis of Ordered Mesoporous Mg-Substituted α-Fe_2O_3

Ordered mesoporous Mg-substituted α-Fe_2O_3 was synthesized by the nanocasting strategy with mesoporous silica KIT-6.[27] Preparation of mesoporous silica KIT-6 was synthesized according to the previous literature.[28] In a typical synthesis, 0.6 g as-prepared mesoporous silica KIT-6 was dispersed in 5 mL toluene and stirred for 30 min, then 1.139 g $Fe(NO_3)_3 \cdot 9H_2O$ and 0.362 g $Mg(NO_3)_2 \cdot 6H_2O$ at an Fe/Mg molar ratio of 2 were added and refluxed for 6 h at 343 K. After refluxing, the resulting mixture was dried in an oven at 333 K overnight and calcined at 873 K for 3 h (heating rate 1 $K \cdot min^{-1}$). Finally, the silica template KIT-6 was dissolved by 2 M NaOH in 333 K under continuously stirring for 24 h, and the red product was produced by washing with distilled water and ethanol and drying at vacuum oven. Pure α-Fe_2O_3 mesoporous sample was also prepared by the same synthetic approach. The conventional Mg-Fe mixed metal oxides without mesoporous structure were prepared by using the traditional solid-phase method, the specific steps are as follows: the corresponding mixture in stoichiometric proportion of $Fe(NO_3)_3 \cdot 9H_2O$ and $Mg(NO_3)_2 \cdot 6H_2O$ were calcined at 873 K for 3 h with a heating rate of 1 $K \cdot min^{-1}$, and the product was denoted as con-Mg/Fe_2O_3.

3. Characterization

Powder X-ray diffraction (XRD) patterns were measured on a Bruker D8 Advance X-ray diffractometer using Cu Kα radiation (λ = 0.154 nm) as X-ray source. The high resolution transmission electron microscopy (HRTEM) images

was collected on Hitachi H-7650 transmission electron microscope with field emission gun at 100 kV. The surface morphology of the solid samples were investigated on a Hitachi S-4800 Scanning Electron Microscopy (SEM). N_2 adsorption-desorption isotherms were measured at 77 K using a Micromeritics Tristar 3000 sorptometer after outgassed at 423 K for a minimum 12 h. The specific surface area and the pore size distribution curves are obtained using the Brunauer-Emmett-Teller (BET) and Barrett-Joyner-Halenda (BJH) methods from the adsorption data. Fourier transform infrared (FT-IR) were performed to assess different functional groups of the materials using KBr pressed disks with a Bruker TENSOR37 FT-IR spectrometer transmission analyzer. X-ray photoelectron spectroscopy (XPS) was recorded on a Kratos ASIS-HS X-ray photoelectronspectroscope with Al Kα source at 150 W (15 kV, 10 mA).

4. Catalytic tests

Catalytic tests were under mild conditions (atmospheric pressure and ~298 K) in a thermostatic reactor of 250 mL continuously stirred. The reaction was performed in kinetic regime and no external and internal diffusional resistances occurred. The initial reaction pH was 7.2 and could be adjusted by adding 0.1 $mol \cdot L^{-1}$ H_2SO_4 to desired pH during the degradation processes. In a typical experiment, 50 mL of MB solution was prepared with an initial concentration of 60 $mg \cdot L^{-1}$, and given amounts of hydrogen peroxide and catalyst were added at reaction time = 0 min. At regular intervals, a 1.0 mL sample was collected in 1.5 mL centrifuge tubes and immediately

mixed with 0.1 mL isopropanol to quench ·OH. It was centrifuged three times (5 min each) at 13,400 rpm to separate catalysts, and the supernatant liquid was collected for analysis.

5. Sample analysis

The concentration of MB in the supernatant liquid was determined at absorbance peak of 664 nm using UV-vis spectrophotometer (UV-752, Shanghai Rex Instrument Co., Ltd., China). ·OH concentration was determined by the terephthalic acid ($C_8H_6O_4$, TA) fluorescence method.[29] Experimental procedure was similar to the measurement of Fenton catalytic activity except that the MB aqueous solution was replaced by the 5×10^{-4} mol·L^{-1} terephthalic acid aqueous solution with a concentration of 2×10^{-3} mol·L^{-1} NaOH. The photoluminescence spectra (PL) of TA samples were obtained by using a Fluorescence Spectrophotometer (F-380, Tianjin Gangdong Instrument Co., Ltd., China.) at room temperature, and the wavelength of excitation was 325 nm. The concentration of Fe (II) ions was determined by reacting the recovered solution after test with 1,10-phenanthroline (maximum of absorption at 510 nm) by a Varian Cary 50 UV-Vis spectrophotometer. Fe (III) concentration was determined by reaction with thiocyanate (maximum of absorption at 480 nm) under acidic conditions.[30] The variation of H_2O_2 concentration during the reaction was analyzed colorimetrically by the same UV-Vis spectrophotometer after complexation with titanium salt.[31]

Result and discussion

1. Characterization of as-prepared samples

In order to investigate the structure-performance relationship of meso-Mg/Fe_2O_3, the morphology of as-prepared catalyst samples was characterized by SEM and the images are shown in Figure 2. It can be seen that the size of these catalyst samples are homogeneous. By comparison between meso-Mg/Fe_2O_3 (Figure 2C and E) and KIT-6 templates (Figure 2A), an increased roughness of catalyst surface in meso-Mg/Fe_2O_3 could be observed. The morphology of meso-Mg/Fe_2O_3 are also very different from meso-Fe_2O_3 and con-Mg/Fe_2O_3 (Figure 2C, B and D). The former still remained the similar surface morphology of KIT-6, and the latter were composed of particles with 200-1000 μm in diameter. After the recycle of the meso-Mg/Fe_2O_3 and con-Mg/Fe_2O_3 (Figure 2E and F), the catalyst particles aggregated and become larger. To further investigate the mesostructure of meso-Mg/Fe_2O_3, representative TEM images of as-synthesized catalyst samples are depicted in Figure 3. From Figure 3A, B and C, the mesoporous structure of meso-Mg/Fe_2O_3 is clearly visible even after the replication of KIT-6.[32, 33] Figure 3D shows clear crystal lattice fringes indicated that meso-Mg/Fe_2O_3 was synthesized with the highly crystalline nature. After the recycle of the meso-Mg/Fe_2O_3 (Figure 3E and 3F), the crystalline nature of catalyst was still remained.[21]

The successful preparation of meso-Mg/Fe_2O_3 is further confirmed by low-angle powder XRD analysis, shown in Figure 4A. The prepared meso-Mg/Fe_2O_3 catalyst

indicated the excellent replica of KIT-6 templates. Mesoporous α-Fe_2O_3 was also in good agreement with the values reported in the literature.[34] Compared with as-made meso-Mg/Fe_2O_3, there was a decrease in intensity of the diffraction peaks for the postreaction meso-Mg/Fe_2O_3, suggesting that the increased hematite particle dispersion, which may be attributed to the decrease in electron density contrast due to the increased Mg leaching during the reaction process.[26] Wide-angle XRD results (including meso-Fe_2O_3, meso-Mg/Fe_2O_3, con-Mg/Fe_2O_3 and postreaction meso-Mg/Fe_2O_3) are shown in Figure 4B. The 2θ values of meso-Mg/Fe_2O_3 at 24.09°, 33.07°, 35.55°, 40.76°, 49.34°, 53.93°, 57.31°, 62.28° and 63.85° could be indexed to the (0 1 2), (1 0 4), (1 1 0), (1 1 3), (0 2 4), (1 1 6), (1 2 2), (2 1 4) and (3 0 0) planes of hexagonal hematite (α-Fe_2O_3, JCPDS No.33-0664). The diffraction pattern for meso-Mg/Fe_2O_3 closely matches the standard α-Fe_2O_3, confirming the success of magnesium substitution to iron in the spinel. The peaks of meso-Mg/Fe_2O_3 are relatively broader than the peaks of con-Mg/Fe_2O_3, which is possibly due to the pore walls were composed of small particles. The average crystallite size of meso-Mg/Fe_2O_3 and postreaction meso-Mg/Fe_2O_3 was determined and calculated to be 7.3 and 5.1 nm, respectively, using the Scherrer equation:

$$D_{hkl} = \frac{0.89\lambda}{\beta_{hkl} \cos \theta_{hkl}}$$

where D_{hkl}, λ, β_{hkl}, and θ_{hkl} were the volume-averaged particle diameter, X-ray wavelength, full width at half maximum (FWHM) and diffraction angle, respectively.

Textural properties of mesoporous catalysts were investigated by N_2 adsorption-desorption measurements, shown in Figure 5. The corresponding

parameters including BET surface area, pore volume and average pore size are listed in Table 1. As shown in Figure 5A, the isotherm of meso-Mg/Fe_2O_3 showed a type IV isotherm at P/P_0 about 0.5, indicating a typical shape of mesoporous materials (Figure 5A). The hysteresis shaping started from about 0.65 and extended almost to 0.95, indicating their large porosity.[35] The specific surface area (90.7 $m^2 \cdot g^{-1}$) and the pore diameter (9.1 nm) are consistent with previous reports on others mesoporous metal oxides, which indicates the successful fabrication of mesoporous Mg/Fe_2O_3.

The surface physico-chemical characteristics of as-prepared catalysts were further explored by FT-IR analysis. According to the infrared active modes polarized to the *c*-axis of the hexagonal crystal system of α-Fe_2O_3, the typical adsorption peaks of α-Fe_2O_3 had a broad absorption at around 560 cm^{-1} and a narrower one at around 480 cm^{-1}.[36, 37] In Figure 6A, the dominant bands of the meso-Mg/Fe_2O_3 (at about 537 cm^{-1} and 471 cm^{-1}) are typical characteristic of crystalline of α-Fe_2O_3. Interestingly, the dominant absorption peak at 568 cm^{-1} of α-Fe_2O_3 shifts to somewhat lower frequencies at 551 cm^{-1} of meso-Fe_2O_3 and 537 cm^{-1} of meso-Mg/Fe_2O_3. Meanwhile, above absorption peak also obviously becomes broader than α-Fe_2O_3 from Figure 6A. It might be due to the changes in the structure of the catalysis, since the catalyst consists of large numbers of small subparticles in the mesoporous structure.[38] Thus, when the average crystallite diameter of subparticles is reduced, the absorption peaks become broader. These results are consistent with XRD and TEM. In Figure 6B, the absorption peak at 540 cm^{-1} of postreaction meso-Mg/Fe_2O_3 hardly changes compared with the one of as-made meso-Mg/Fe_2O_3, suggesting that the catalyst has not been

affected in our experimental conditions.

2. Efficient MB degradation performance in the presence of meso-Mg/Fe_2O_3

In the previous studies, α-Fe_2O_3 has been proven to be an easily recyclable and efficient catalyst for the degradation of MB, so control experiments for meso-Mg/Fe_2O_3-H_2O_2-MB system was evaluated.[39, 40] The external and internal diffusional resistances of the degradation processes were excluded, and the reaction was performed in kinetic regime before the analysis. Prior to the addition of H_2O_2, the mixed solution of MB and the catalysts was stirred in the dark for 30 min to establish the equilibrium adsorption state.[26]

A series of experiments were performed by varying the catalyst loading of meso-Mg/Fe_2O_3 from 0.2 g·L^{-1} to 0.6 g·L^{-1} and the result was depicted in Figure 7A. From Figure 7A, the degradation efficiency increased with the meso-Mg/Fe_2O_3 catalyst loading. At 0.6 g·L^{-1} of meso-Mg/Fe_2O_3, MB degradation reached almost 98 % in 180 min[41] Moreover, the data for MB concentration decay were further analyzed by the first order kinetic equation, which could be expressed as

$$\mathrm{In}\left(\frac{C_0}{C}\right) = k't$$

where k' is the apparent reaction constant and C_0 and C are the initial concentration and the concentration at time t, of MB, respectively. The degradation of MB follows the pseudo-first order reaction kinetics.The apparent rate constant of used meso-Mg/Fe_2O_3 is 1.972 h^{-1}, which is 1.22, 3.02 and 4.53 times than those of meso-Fe_2O_3, con-Mg/Fe_2O_3 and α-Fe_2O_3. The rate constant k' increased linearly with

increasing catalyst dosage (see Figure 7B and 7C).

During the heterogeneous Fenton degradation of MB, it should be noted that the adsorption of MB by meso-Mg/Fe_2O_3 could achieve about 9 % (Figure 7A, curve (a)), which is due tothe high specific surface area of meso-Mg/Fe_2O_3 (90.7 $m^2 \cdot g^{-1}$). The experiment in homogeneous systems was also performed. After vigorous agitation for 4 h, meso-Mg/Fe_2O_3 catalyst was removed and H_2O_2 was added into the clear filtrate (380 μL, 30 wt.%). As shown in Figure 7A and 8A, the removal of MB by adsorption was 9 %, the removal of MB by pure H_2O_2 at 6 h was 12 %, while the removal of MB catalyzed by leaching Fe ions (concentration ~5 $mg \cdot L^{-1}$) was 25 %. Therefore, the contribution of homogeneous Fenton reaction was 3 %. The results of this experiment clearly indicate that the production of hydroxyl radicals observed primarily occurs at the nanoparticle surface rather than being catalyzed by the Fe ions leached into the filtrate. To accurately estimate the catalytic activity of meso-Mg/Fe_2O_3, comparable amounts of $FeSO_4$ (Fe ions concentration 60 $mg \cdot L^{-1}$) was used to catalyze the degradation of MB. The results show that 60 $mg \cdot L^{-1}$ MB could be completely degraded in 30 min (Figure 8A). These results indicated that the contribution of Fenton-like reaction was mainly dominated by the meso-Mg/Fe_2O_3 catalysts. From Figure 8B, four kinds of catalysts with the same Fe loading display distinctly different catalytic activities (meso-Mg/Fe_2O_3> meso-Fe_2O_3> con-Mg/Fe_2O_3> α-Fe_2O_3). The excellent catalytic activity of mesoporous catalysts is strongly originated from ordered mesoporous network structure and large pore size, which contributed to the raised numbers of accessible active sites of the catalysts and increased mass transfer of MB

in the catalysts porosity.[42]

It is well known that the pH value is one of most significant factors in the Fenton reaction system.[43, 44] Investigation and extension of pH range on the performance of heterogeneous Fenton-like catalyst is of crucial importance for the development of new heterogeneous Fenton-like process.[16] As shown in Figure 9, the initial rate was relatively slow at pH 3.5, and then it followed a fast degradation rate. In case of pH 7.5, the rate of reaction was very fast and the conversion of MB was 98 % over a period of 180 min. The results indicated that the reaction performance could be highest at around pH 7.5 and decreased with increasing pH. Generally, the homogeneous Fenton system shows best performance at pH ≈ 3.[45] At neutral even higher pH, formation of $Fe(OH)_3$ precipitate (pK_{sp} = 37.4) prevents the catalysis reaction proceeding. However, the addition of Mg into heterogeneous Fenton catalysts could expand its degradation pH range during the reaction processes. The substitution of Mg on heterogeneous Fenton catalysts makes the slightly acidic surface of catalysts become slightly basic.[26] And these basic sites on the catalyst surface can promote the formation of the surface Fe-OH complex, which is crucial to activating H_2O_2.[46, 47] Therefore, compared with conventional Fenton reaction, meso-Mg/Fe_2O_3 could also be used over a wide pH range.

The remained TOC after total MB degradation with different catalyst could be attributed to organic acids accumulated in the solution (Figure 10). It can be observed that pure H_2O_2 and α-Fe_2O_3 did not produce a significant TOC reduction. Con-Mg/Fe_2O_3 and meso-Fe_2O_3 showed 22 % and 31 % TOC reduction, respectively.

On the other hand, meso-Mg/Fe_2O_3 produced the highest TOC reduction of about 54 % after 280 min reaction. In order to identify the end products, degraded samples of MB were analyzed by ion exclusion chromatography (results not reported). Oxalic acid and formic acid were identified as byproducts of the aromatic ring cleavage and often detected after degradation of MB.[43]

In order to compare the effect of the ·OH radicals concentration of meso-Mg/Fe_2O_3-H_2O_2 Fenton system, the dependence of the ·OH radicals concentration of H_2O_2 over different heterogeneous Fenton catalysts is researched under the same conditions. The generated ·OH radicals in the catalytic process was investigated according to the reaction ·OH and terephthalic acid producing 2-hydroxyterephthalic acid. The PL intensity at 425 nm gradually rises with increasing irradiation time in the presence of different catalysts (Figure 11). From Figure 11D, the ·OH intensity of meso-Mg/Fe_2O_3 is higher than that of the individual meso-Fe_2O_3 and con-Mg/Fe_2O_3. Therefore, degradation activity of the meso-Mg/Fe_2O_3 could also be expected to be higher than that of meso-Fe_2O_3 and con-Mg/Fe_2O_3. Above results also account for the higher catalytic activity of meso-Mg/Fe_2O_3 in comparison with that of α-Fe_2O_3. From Figure 11C, generation rates of ·OH radicals in con-Mg/Fe_2O_3 and meso-Mg/Fe_2O_3 were slower than that of α-Fe_2O_3 and meso-Fe_2O_3 at the beginning of the reaction. After 60 min, in a sharp contrast, above Mg-substituted samples (especially meso-Mg/Fe_2O_3) showed a much higher generation rates compared to the pure α-Fe_2O_3 and meso-Fe_2O_3. This indicates that the initial surface structure of the as-made catalyst plays a critical role at the

beginning of the reaction. However, if the reaction time is long enough, the meso-Mg/Fe_2O_3 catalyst experienced the Mg leaching under catalytic environment. The departure of Mg cations from catalysts could create defects or vacancies in the meso-Mg/Fe_2O_3 structure, and therefore activate the catalyst.[27] A more stable surface of the catalyst formed for prolonged catalytic oxidation, leading to the increasing of the catalyst activity (shown in Table 1).[21] The leaching process is slow and could not be observed in a short reaction time (30 min). The leaching/activation mechanism could be summarized in Figure 1.

In order to clarify the origin of the difference in activities, detailed structural characterizations of meso-Mg/Fe_2O_3 were studied before and after the degradation of MB. The chemical composition of meso-Mg/Fe_2O_3 and related catalysts was confirmed by ICP-AES, and the Mg/Fe molar ratio was shown in Table 1. From Table 1, the Mg/Fe molar ratio was reduced to 0.14 compared to the initial Mg/Fe ratio of 0.59. The postreaction meso-Mg/Fe_2O_3 exhibited typical isotherms for traditional ordered mesoporous materials and a much higher BET surface area (190.4 $m^2 \cdot g^{-1}$) than the as-made catalyst (90.7 $m^2 \cdot g^{-1}$). Thus, the Mg leaching during the reaction processes increases the surface area of meso-Mg/Fe_2O_3 by approximately 100 $m^2 \cdot g^{-1}$. To verify the contributions of Mg cations to the increased surface area, the as-made meso-Mg/Fe_2O_3 and meso-Fe_2O_3 were treated in diluted aqueous HNO_3 solution (pH = 3) for 30 min and investigated by N_2 adsorption measurements. The BET surface areas for acid-treated meso-Mg/Fe_2O_3 and meso-Fe_2O_3 are 203.9 $m^2 \cdot g^{-1}$ and 103.7 $m^2 \cdot g^{-1}$, respectively. These results are consistent with our conclusion that the Mg

leaching contributes ~100 $m^2 \cdot g^{-1}$ surface area. The departure of Mg cations from mesoporous Fe_2O_3 surface may create defects or vacancies in the iron oxide surface and leads to a highly porous structure.[27]

XPS analysis of meso-Mg/Fe_2O_3 were carried out to better understand the roles of iron and magnesium in Fenton-like catalytic oxidation. (shown in Figure 12). The O1s core level spectrum shows the dominant oxide peaks at round 530.1 eV, which are in good agreement with the literature values of α-Fe_2O_3.[48] In the meso-Mg/Fe_2O_3 and postreaction meso-Mg/Fe_2O_3 catalysts, this peak practically disappears, and shifted to 531.7 eV and 530.8 eV. During the heterogeneous Fenton oxidation processes, the Mg ions were removed from the meso-Mg/Fe_2O_3 structure. The departure of Mg cations from catalyst structure may prompt the O1s peak of meso-Mg/Fe_2O_3 gradually close to the peak of pure α-Fe_2O_3 due to strong interaction between Fe^{3+} and related metal oxides. A very complex line-shape is observed in the Fe2p spectra (Figure 12B) of the same catalysts. As expected, the typical photoelectron peaks at 711 and 725 eV are the characteristic doublets of $Fe^{3+}2p_{3/2}$ and $Fe^{3+}2p_{1/2}$ core-level spectra of α-Fe_2O_3. On the other hand, the spectra of meso-Mg/Fe_2O_3 and postreaction meso-Mg/Fe_2O_3 were fitted with six contributions.[4] The peaks at 724.5 eV and 711.1 eV in the meso-Mg/Fe_2O_3 are assigned to $Fe^{3+}2p_{3/2}$ and $Fe^{3+}2p_{1/2}$, suggesting the presence of Fe^{3+} cations. The other peaks are due to shake-up satellites of the $2p_{3/2}$ and $2p_{1/2}$ peaks. In postreaction meso-Mg/Fe_2O_3, the $Fe^{3+}2p_{3/2}$ and $Fe^{3+}2p_{1/2}$ peaks are shifted to 724.1 eV and 710.7 eV, respectively, due to the interaction between the clusters of iron oxides and related oxides. And the Fe2p peaks were gradually close to the peaks of

pure α-Fe_2O_3, indicating the valence of Fe was not changed and its impact on Fe was gradually reduced with the leaching of Mg cations.

Once mesoporous α-Fe_2O_3 fabricated through substitution and selective leaching of magnesium, a highly porous mesoporous Mg modified Fe_2O_3 with a significant amount of defects was made. The catalyst showed an enhanced activity in the MB degradation under mild conditions. Based on the experimental results of the XPS and the measured amount of ·OH radicals, a plausible mechanism related to the active ·OH radicals in the meso-Mg/Fe_2O_3 system is proposed. Firstly, MB was adsorbed on the surface of meso-Mg/Fe_2O_3. Once H_2O_2 was added, Fe(III) initiated H_2O_2 decomposition started from the reduction of Fe(III) and the formation of HO_2· (O_2·$^-$). ThenOH radicalsand reduced Fe(II) species generated according to the Haber-Weiss mechanism.[49, 50] Then the·OH radicals reacted with MB both adsorbed on the catalyst surface and dissolved in the bulk solution, leading to the further degradation and mineralization of pollutants. Nevertheless, the decomposing H_2O_2 to generate ·OH radical can be described in the following reactions:[18]

$$\equiv Fe(III) + H_2O_2 \rightarrow \equiv Fe(III)(H_2O_2)_{ads} \quad (1)$$

$$\equiv Fe(III)(H_2O_2)_{ads} \rightarrow \equiv Fe(II) + HO_2\cdot + H^+ \quad (2)$$

$$\equiv Fe(II) + H_2O_2 \rightarrow \equiv Fe(III) + \cdot OH + OH^- \quad (3)$$

Worth noting that, at pH ≥ 4 in a heterogeneous system, the catalytic reaction mainly occurs on the catalyst surface. Therefore, the adsorption of H_2O_2 onto the metal centers plays an important role in this heterogeneous Fenton-like reaction. In the case of meso-Mg/Fe_2O_3, the surface nature of Mg is also highly hydroxylated,

which can facilitate the formation of the surface ·OH complexes.[46, 51] This is crucial for adsorption of H_2O_2 and consequently contributes to a more rapid performance of the oxidation processes.[47] Meanwhile, MB hardly degraded in the presence of dissolved Mg^{2+} ions and H_2O_2, which indicating that Mg^{2+} ions is not responsible for the MB degradation. Hence, a much better catalytic activity of meso-Mg/Fe_2O_3 compared with meso-Fe_2O_3 was ascribed to the synergetic effects of the desirable basic sites on the surface of the Mg and increased BET surface area and broader pore size distributions.

3. Excellent chemical reusability and stability of meso-Mg/Fe_2O_3 catalyst

Figure 13 shows the MB degradation on the meso-Mg/Fe_2O_3 in three different batch runs. After each run, the catalyst was recovered by filtration and washed by deionized water and dried at 80 °C overnight. It was noteworthy that the activity of meso-Mg/Fe_2O_3 was increased after regeneration. For mesoporous α-Fe_2O_3 is the active component for heterogeneous Fenton-like reactions, substitution of Fe with alkaline metal will significantly decrease the activity at first batch run. Then, with the leaching of Mg and surface restructuring under catalytic environment, the Mg-substituted catalysts (especially meso-Mg/Fe_2O_3) were activated (Enlarged part of Figure 13).[27] This indicates that meso-Mg/Fe_2O_3 possesses enhanced chemical and catalytic stability. Notably, with the increase of reusability of meso-Mg/Fe_2O_3 catalyst, both the leaching concentration of Mg and the catalytic activity of the catalyst increased, which is quite different with the catalytic mechanism of composite

components in heterogeneous Fenton processes, such as Fe-Cu and Fe-Zn composites.[23, 24] The addition of Cu^{2+} is thermodynamically favorable the reduction of Fe^{3+}, which is benefit for the redox cycles of Fe^{2+}/Fe^{3+} and even for regeneration of the active species Fe^{2+}. In meso-Mg/Fe_2O_3-H_2O_2-MB system, approximately two thirds of Mg cations were removed in the leaching/activating process. Especially, the meso-Mg/Fe_2O_3 with unique mesoporous structure possesses ultrahigh surface area and enlarged pore size, which effectively reduced the mass transfer resistance and enhanced the number of active sites of the catalyst.

The stability of the catalyst was also evaluated under the reaction conditions of meso-Mg/Fe_2O_3-H_2O_2-MB system. Table 2 shows the influence of pH, H_2O_2 concentration, catalyst dosage and reusage on dissolved iron concentrations during the reactions. It can be seen that the dissolved iron species increased from 3.45 $mg \cdot L^{-1}$ to 6.72 $mg \cdot L^{-1}$ after 3 h when the pH decreased from 7.5 to 2.0. Also shown in Table 2, dissolved iron species increased from 3.17 $mg \cdot L^{-1}$ to 4.53 $mg \cdot L^{-1}$ after 3 h reaction when H_2O_2 concentration increased from 1600 $mg \cdot L^{-1}$ to 4600 $mg \cdot L^{-1}$ at initial pH 7.5.[52, 53] The leaching concentration of Mg decreased after second and third cycles, which indicates that the Mg cations in the meso-Mg/Fe_2O_3 also reduced. Magnesium is essential element required by human body. It is not regulated in aqueous environment, which implied that the Mg ions leached from the meso-Mg/Fe_2O_3 catalyst will not result in the extra environmental and health problems. The treated waste water could be directly discharged into the sewage system.

Conclusions

The ordered mesoporous magnesium-substituted α-Fe_2O_3 (meso-Mg/Fe_2O_3) was successfully synthesized by using KIT-6 as template through the hard templating strategy. The texture, morphology and structure of the meso-Mg/Fe_2O_3 catalyst before and after degradation of MB were characterized by SEM, HRTEM, XRD, N_2 adsorption-desorption, FT-IR and XPS analysis. The pseudo-first order reaction kinetics was fitted well to all experiments. With the increase of reusability of meso-Mg/Fe_2O_3 catalyst, both the leaching concentration of Mg and the catalytic activity of the catalyst increased, which is quite different with the catalytic mechanism of composite components in heterogeneous Fenton-like processes, such as Fe-Cu and Fe-Zn composites. The postreaction meso-Mg/Fe_2O_3 showed a much higher BET surface area and broader pore size distribution than the as-made sample, which is likely due to Mg leaching during the Fenton-like catalysis process. The structural framework of as-prepared catalyst was not changed during the reaction. In addition, the released amounts of Fe were found to be low. Hence, meso-Mg/Fe_2O_3 catalyst has proved to have a unique and superb catalytic activity in the heterogeneous Fenton-like system and it will be an attractive alternative in the treatment of environmental problems.

Acknowledgments

This work was supported by the National Natural Science Foundation of China, NSFC (21101113, 51172157, 51202159, 51208357, 51472179), Doctoral Program of

Higher Education, Ministry of Education (20120032120017), Municipal Natural Science Foundation of Tianjin (13JCYBJC16900, 13JCQNJC08200).

References

1. C. L. Yap, S. Gan and H. K. Ng, *Chemosphere*, 2011, **83**, 1414-1430.

2. X. Zhang, M. Lin, X. Lin, C. Zhang, H. Wei, H. Zhang and B. Yang, *ACS Appl. Mater. Interfaces*, 2014, **6**, 450-458.

3. M. C. Pereira, L. C. A. Oliveira and E. Murad, *Clay Miner.*, 2012, **47**, 285-302.

4. J. V. Coelho, M. S. Guedes, R. G. Prado, J. Tronto, J. D. Ardisson, M. C. Pereira and L. C. A. Oliyeira, *Appl. Catal. B-Environ.*, 2014, **144**, 792-799.

5. A. Dhakshinamoorthy, S. Navalon, M. Alvaro and H. Garcia, *ChemSusChem*, 2012, **5**, 46-64.

6. A. D. Bokare and W. Choi, *J. Hazard. Mater.*, 2014, **275**, 121-135.

7. S. Navalon, A. Dhakshinamoorthy, M. Alvaro and H. Garcia, *ChemSusChem*, 2011, **4**, 1712-1730.

8. L. Zhou, Y. Shao, J. Liu, Z. Ye, H. Zhang, J. Ma, Y. Jia, W. Gao and Y. Li, *ACS Appl. Mater. Interfaces*, 2014, **6**, 7275-7285.

9. C. Liu, J. Li, J. Qi, J. Wang, R. Luo, J. Shen, X. Sun, W. Han and L. Wang, *ACS Appl. Mater. Interfaces*, 2014, **6**, 13167-13173.

10. Y. Wang, G. Zhao, S. Chai, H. Zhao and Y. Wang, *ACS Appl. Mater. Interfaces*, 2013, **5**, 842-852.

11. M. Muruganandham, R. P. S. Suri, M. Sillanpaa, J. J. Wu, B. Ahmmad, S. Balachandran and M. Swaminathan, *J. Nanosci. Nanotechnol.*, 2014, **14**, 1898-1910.

12. X. J. Yang, X. M. Xu, J. Xu and Y. F. Han, *J. Am. Chem. Soc.*, 2013, **135**,

16058-16061.

13. S. R. Pouran, A. A. A. Raman and W. M. A. W. Daud, *J. Cleaner Prod.*, 2014, **64**, 24-35.

14. F. X. Bu, M. Hu, L. Xu, Q. Meng, G. Y. Mao, D. M. Jiang and J. S. Jiang, *Chem. Commun.*, 2014, **50**, 8543-8546.

15. T. Zeng, X. Zhang, S. Wang, Y. Ma, H. Niu and Y. Cai, *Chem.-Eur. J.*, 2014, **20**, 6474-6481.

16. S. Navalon, M. Alvaro and H. Garcia, *Appl. Catal. B-Environ.*, 2010, **99**, 1-26.

17. C. Cornu, J. L. Bonardet, S. Casale, A. Davidson, S. Abramson, G. Andre, F. Porcher, I. Grcic, V. Tomasic, D. Vujevic and N. Koprivanac, *J. Phys. Chem. C*, 2012, **116**, 3437-3448.

18. M. Xia, M. Long, Y. Yang, C. Chen, W. Cai and B. Zhou, *Appl. Catal. B-Environ.*, 2011, **110**, 118-125.

19. J. Shi, Z. Ai and L. Zhang, *Water Res.*, 2014, **59**, 145-153.

20. M. Zhang, Q. Yao, W. Guan, C. Lu and J. M. Lin, *J. Phys. Chem. C*, 2014, **118**, 10441-10447.

21. A. H. Lu and F. Schueth, *Adv. Mater.*, 2006, **18**, 1793-1805.

22. P. D. Yang, D. Y. Zhao, D. I. Margolese, B. F. Chmelka and G. D. Stucky, *Nature*, 1998, **396**, 152-155.

23. Y. Wang, H. Zhao, M. Li, J. Fan and G. Zhao, *Appl. Catal. B*, 2014, **147**, 534-545.

24. M. Su, C. He, V. K. Sharma, M. A. Asi, D. Xia, X. Z. Li, H. Deng and Y. Xiong, *J. Hazard. Mater.*, 2012, **211**, 95-103.

25. M. Hartmann, S. Kullmann and H. Keller, *J. Mater. Chem.*, 2010, **20**, 9002-9017.

26. L. Hu, F. Yang, W. Lu, Y. Hao and H. Yuan, *Appl. Catal. B*, 2013, **134**, 7-18.

27. J. Rosen, G. S. Hutchings and F. Jiao, *J. Am. Chem. Soc.*, 2013, **135**, 4516-4521.

28. M. Choi, K. Na, J. Kim, Y. Sakamoto, O. Terasaki and R. Ryoo, *Nature*, 2009, **461**, 246-U120.

29. K. Ishibashi, A. Fujishima, T. Watanabe and K. Hashimoto, *J. Photochem. Photobiol. A,* 2000, **134**, 139-142.

30. H. Tamura, K. Goto, T. Yotsuyanagi and M. Nagayama, *Talanta*, 1974, **21**, 314-318.

31. J. De Laat and H. Gallard, *Environ. Sci. Technol.*, 1999, **33**, 2726-2732.

32. X. Sun, Y. Shi, P. Zhang, C. Zheng, X. Zheng, F. Zhang, Y. Zhang, N. Guan, D. Zhao and G. D. Stucky, *J. Am. Chem. Soc.*, 2011, **133**, 14542-14545.

33. H. F. Yang and D. Y. Zhao, *J. Mater. Chem.*, 2005, **15**, 1217-1231.

34. W. Yue and W. Zhou, *Chem. Mat.*, 2007, **19**, 2359-2363.

35. N. Najmoddin, A. Beitollahi, M. Muhammed, N. Ansari, E. Devlin, S. M. Mohseni, H. Rezaie, D. Niarchos, J. Akerman and M. S. Toprak, *J. Alloys Compd.*, 2014, **598**, 191-197.

36. A. L. Andrade, D. M. Souza, M. C. Pereira, J. D. Fabris and R. Z. Domingues, *J. Nanosci. Nanotechnol.*, 2009, **9**, 3695-3699.

37. Y. S. Wang, A. Muramatsu and T. Sugimoto, *Colloid Surf. A*, 1998, **134**, 281-297.

38. Z. Jing, S. H. Wu., S. M. Zhang, and W. P. Huang, *Mater. Res. Bull.*, 2004, **39**, 2057-2064.

39. I. Ursachi, A. Stancu and A. Vasile, *J. Colloid Interface Sci.*, 2012, **377**, 184-190.

40. Y. Liu, H. Yu, S. Zhan, Y. Li, Z. Lv, X. Yang and Y. Yu, *J. Sol-Gel Sci. Technol.*, 2011, **58**, 716-723.

41. C. Bai, W. Gong, D. Feng, M. Xian, Q. Zhou, S. Chen, Z. Ge and Y. Zhou, *Chem. Eng. J.*, 2012, **197**, 306-313.

42. X. Zhong, J. Barbier, Jr., D. Duprez, H. Zhang and S. Royer, *Appl. Catal. B*, 2012, **121**, 123-134.

43. J. L. Wang and L. J. Xu, *Crit. Rev. Environ. Sci. Technol.*, 2012, **42**, 251-325.

44. V. K. Gupta, I. Ali, T. A. Saleh, A. Nayak and S. Agarwal, *RSC Adv.*, 2012, **2**, 6380-6388.

45. J. Herney-Ramirez, M. A. Vicente and L. M. Madeira, *Appl. Catal. B*, 2010, **98**, 10-26.

46. Q. Yang, H. Choi, S. R. Al-Abed and D. D. Dionysiou, *Appl. Catal. B*, 2009, **88**, 462-469.

47. M. Stoyanova, I. Slavova, S. Christoskova and V. Ivanova, *Appl. Catal. A*, 2014, **476**, 121-132.

48. L. Li, Y. Chu, Y. Liu and L. Dong, *J. Phys. Chem. C*, 2007, **111**, 2123-2127.

49. W. P. Kwan and B. M. Voelker, *Environ. Sci. Technol.*, 2003, **37**, 1150-1158.

50. S. S. Lin and M. D. Gurol, *Environ. Sci. Technol.*, 1998, **32**, 1417-1423.

51. W. Zhang, H. L. Tay, S. S. Lim, Y. Wang, Z. Zhong and R. Xu, *Appl. Catal. B*, 2010, **95**, 93-99.

52. J. H. Ramirez, F. J. Maldonado-Hodar, A. F. Perez-Cadenas, C. Moreno-Castilla,

C. A. Costa and L. M. Madeira, *Appl. Catal. B*, 2007, **75**, 312-323.

53. X. Hu, B. Liu, Y. Deng, H. Chen, S. Luo, C. Sun, P. Yang and S. Yang, *Appl. Catal. B*, 2011, **107**, 274-283.

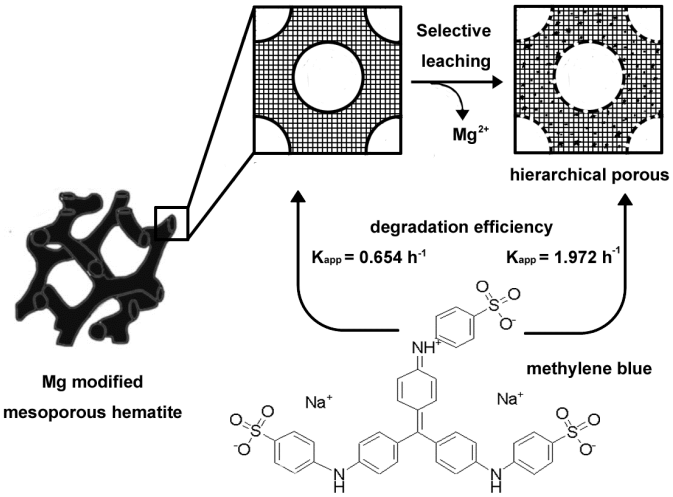

Figure 1. Schematic illustration of mesoporous Mg-Fe_2O_3 through Mg ions leaching.

Arrows show the Mg leaching sites (i.e., defect sites).

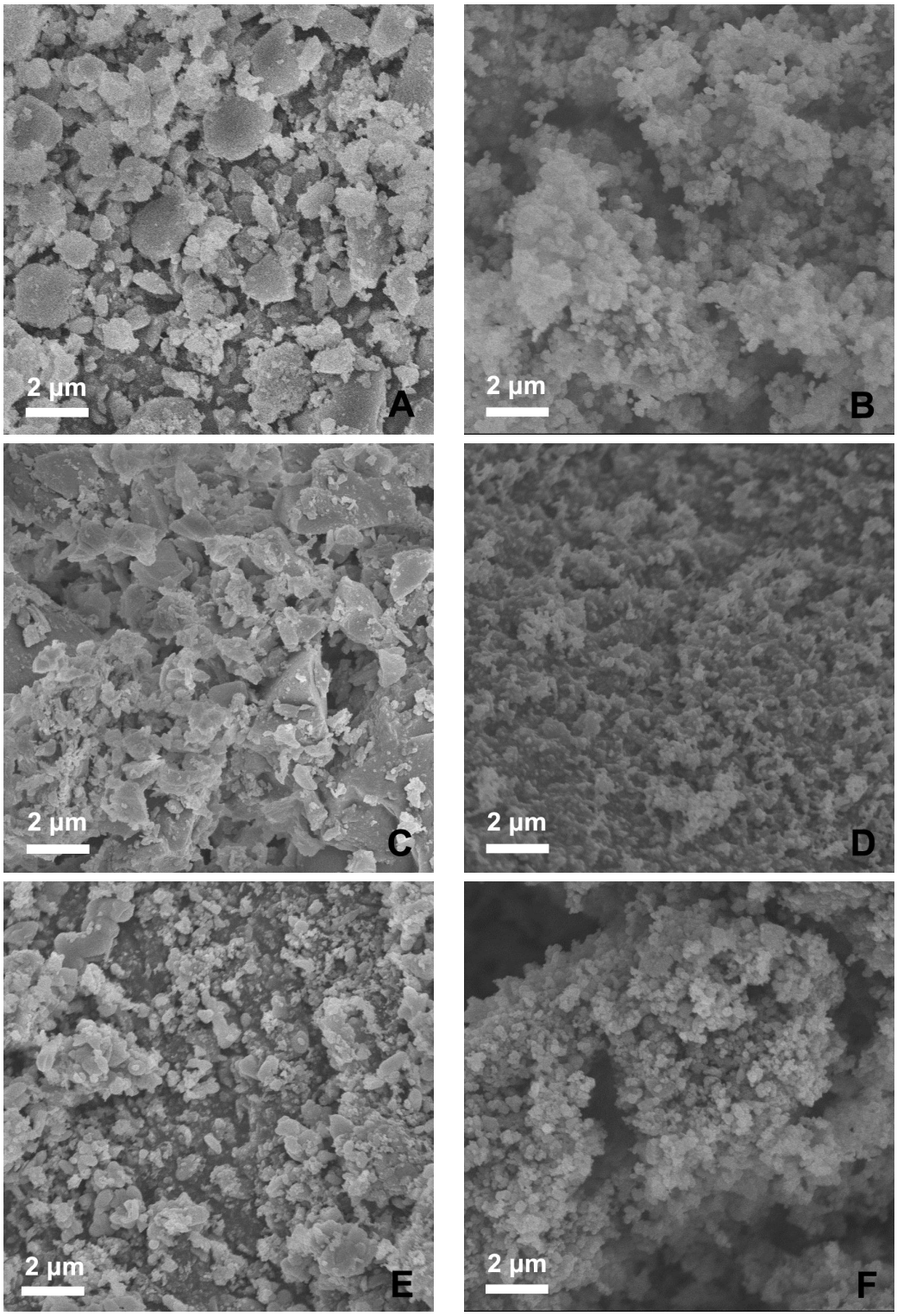

Figure 2. SEM images of KIT-6 (A), meso-Fe_2O_3 (B), meso-Mg/Fe_2O_3 (C), con-Mg/Fe_2O_3 (D), postreaction meso-Mg/Fe_2O_3 (E) and postreaction con-Mg/Fe_2O_3 (F).

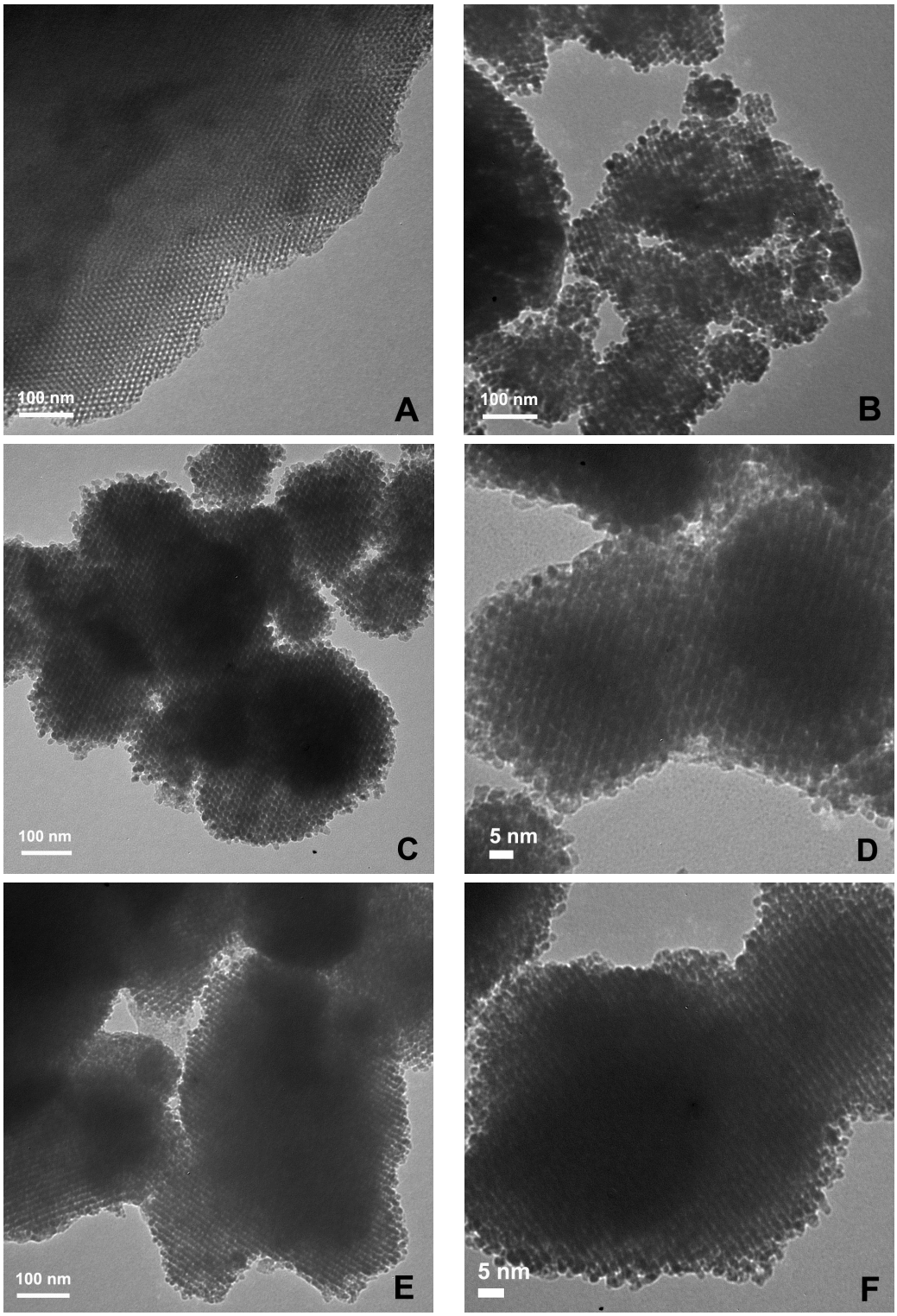

Figure 3. TEM images of KIT-6 (A), meso-Fe_2O_3 (B), meso-Mg/Fe_2O_3 (C), high resolution meso-Mg/Fe_2O_3 (D), postreaction meso-Mg/Fe_2O_3 (E) and high resolution postreaction meso-Mg/Fe_2O_3 (F).

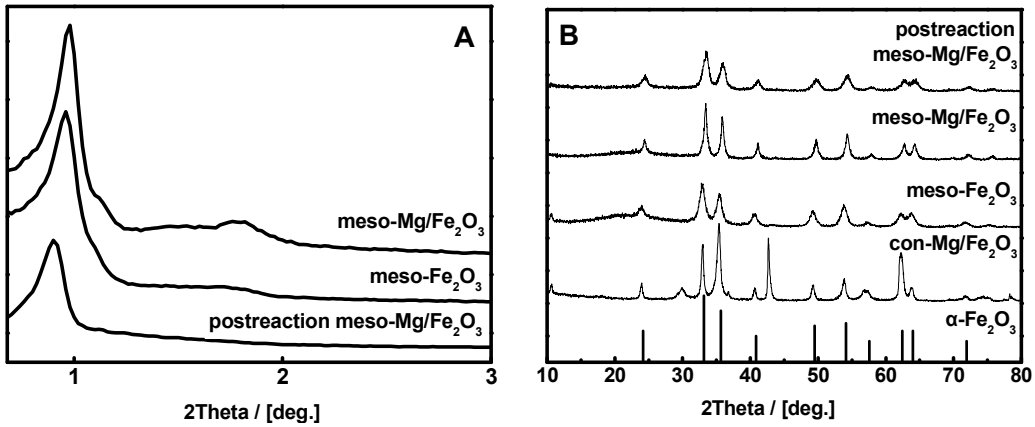

Figure 4. (A) Low-angle XRD patterns of meso-Fe_2O_3, meso-Mg/Fe_2O_3 and postreaction meso-Mg/Fe_2O_3; (B) high-angle XRD patterns of α-Fe_2O_3, con-Mg/Fe_2O_3, meso-Fe_2O_3, meso-Mg/Fe_2O_3 and postreaction meso-Mg/Fe_2O_3.

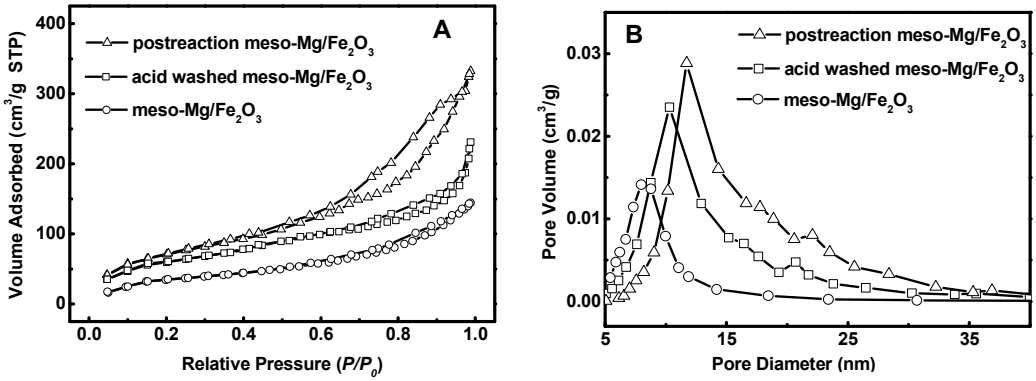

Figure 5. (A) N_2 adsorption-desorption isotherms for meso-Mg/Fe_2O_3, acid washed meso-Mg/Fe_2O_3 and postreaction meso-Mg/Fe_2O_3; (B) pore size distributions from the desorption branches through the BJH method for meso-Mg/Fe_2O_3, acid washed meso-Mg/Fe_2O_3 and postreaction meso-Mg/Fe_2O_3.

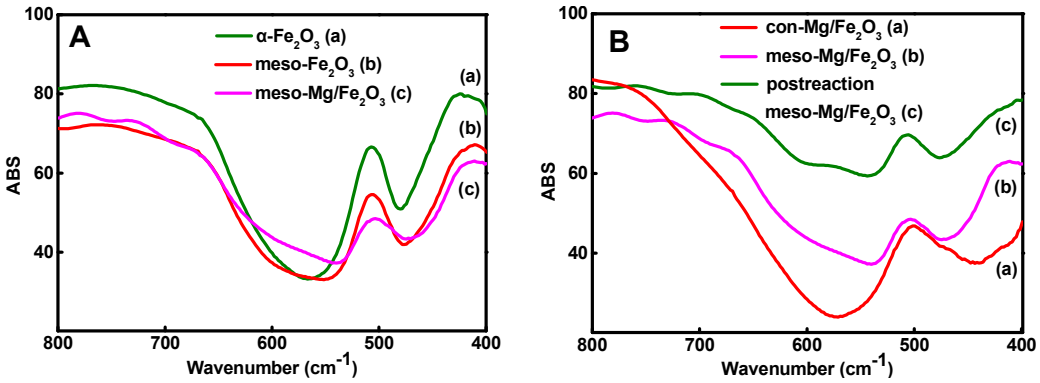

Figure 6. FT-IR spectra of (A) bulk Fe_2O_3, meso-Fe_2O_3, meso-Mg/Fe_2O_3, con-Mg/Fe_2O_3, and (B) con-Mg/Fe_2O_3, meso-Mg/Fe_2O_3 and postreaction meso-Mg/Fe_2O_3. (For interpretation of the references to color in this figure legend, the reader is referred to the web version of this article.)

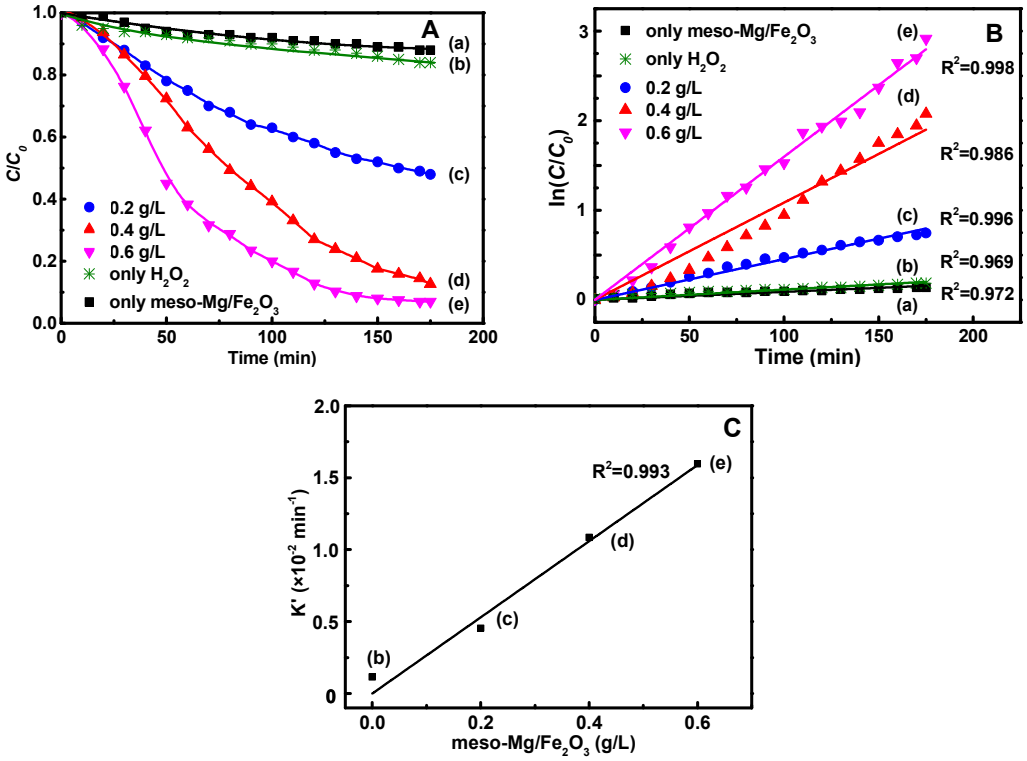

Figure 7. (A) The removal efficiency of methylene blue in the presence of meso-Mg/Fe_2O_3 0.4 $g \cdot L^{-1}$ (a), H_2O_2 (2600 $mg \cdot L^{-1}$) (b), meso-Mg/Fe_2O_3 (0.2 $g \cdot L^{-1}$) + H_2O_2 (c), meso-Mg/Fe_2O_3 (0.4 $g \cdot L^{-1}$) + H_2O_2 (d) and meso-Mg/Fe_2O_3 (0.6 $g \cdot L^{-1}$) + H_2O_2 (e); (B) the kinetic curves of methylene blue degradation on the dependence of $\ln(C/C_0)$ versus time; (C) the kinetic analysis of methylene blue degradation on the dependence of meso-Mg/Fe_2O_3 catalyst loading. (initial pH, H_2O_2 dosage = 2600 $mg \cdot L^{-1}$ and initial MB concentration = 60 $mg \cdot L^{-1}$).

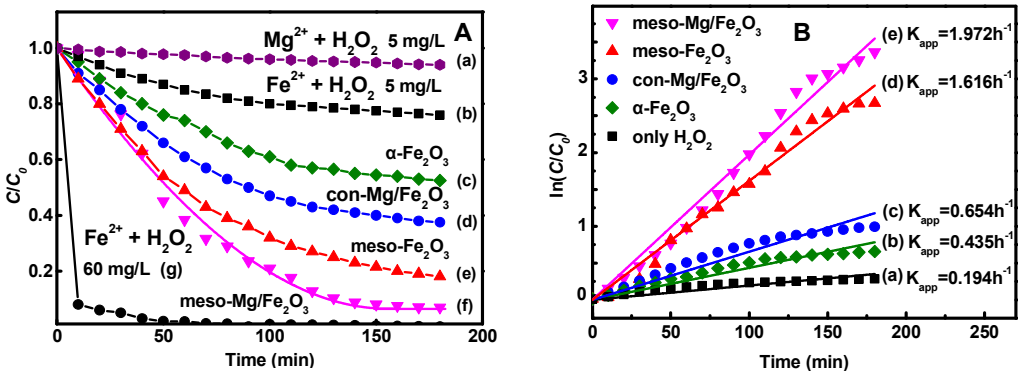

Figure 8. (A) The degradation efficiency of methylene blue with different catalyst during the reaction. Homogeneous Mg^{2+} (5 mg·L^{-1}) (a), homogeneous Fe^{2+} (5 mg·L^{-1}) (b), α-Fe_2O_3 (c), con-Mg/Fe_2O_3 (d), meso-Fe_2O_3 (e), meso-Mg/Fe_2O_3 (0.6 g·L^{-1}) (f) and homogeneous Fe^{2+} (60 mg·L^{-1}) (g); (B) the kinetic curves of methylene blue degradation on the dependence of ln(C/C_0) versus time. (initial pH, H_2O_2 dosage= 2600 mg·L^{-1} and initial MB concentration = 60 mg·L^{-1}).

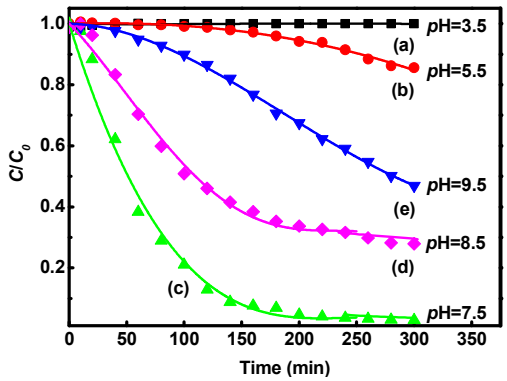

Figure 9. Effect of initial pH on degradation of methylene blue with Mg/Fe_2O_3 suspensions: pH 3.5 (a), pH 5.5 (b), pH 7.5 (c), pH 8.5 (d) and pH 9.5 (e). (H_2O_2 dosage= 2600 $mg \cdot L^{-1}$, initial MB concentration = 60 $mg \cdot L^{-1}$ and catalyst dosage= 0.6 $g \cdot L^{-1}$).

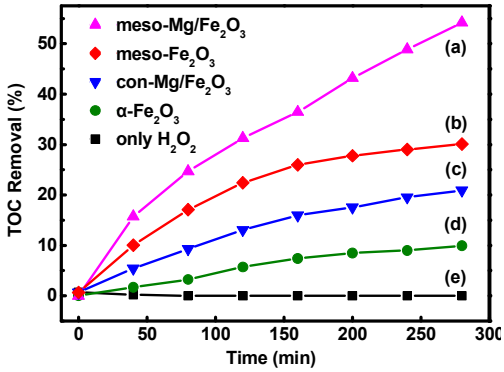

Figure 10. Temporal changes of TOC during the degradation of methylene blue with different catalyst. H_2O_2 (2600 mg·L^{-1}) (a), α-Fe_2O_3 (b), con-Mg/Fe_2O_3 (c), meso-Fe_2O_3 (d) and meso-Mg/Fe_2O_3 (0.6 g·L^{-1}) (e). (initial pH, H_2O_2 dosage= 2600 mg·L^{-1} and initial MB concentration = 60 mg·L^{-1}).

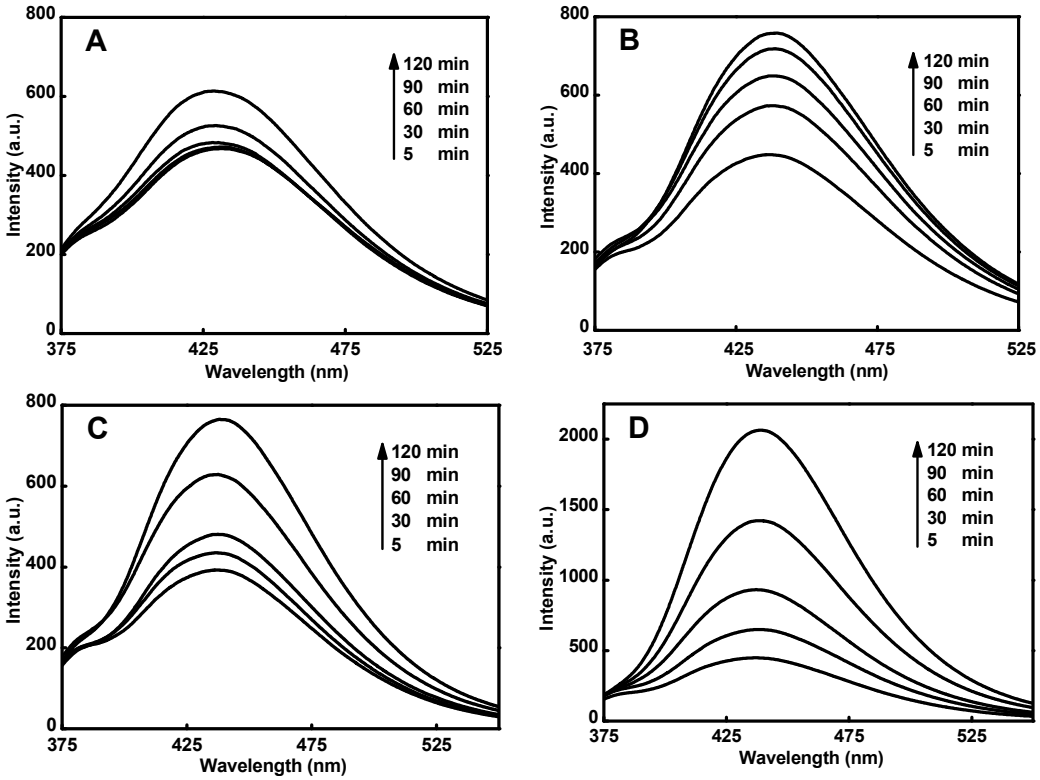

Figure 11. Total concentrations of ·OH formed as a function of time. α-Fe_2O_3 (A), meso-Fe_2O_3 (B), con-Mg/Fe_2O_3 (C) and meso-Mg/Fe_2O_3 (D). (pH = 3.00, H_2O_2 dosage= 1300 mg·L^{-1}, catalyst dosage = 0.3 g L^{-1} and benzoic acid used as a probe at 1200 mg·L^{-1}).

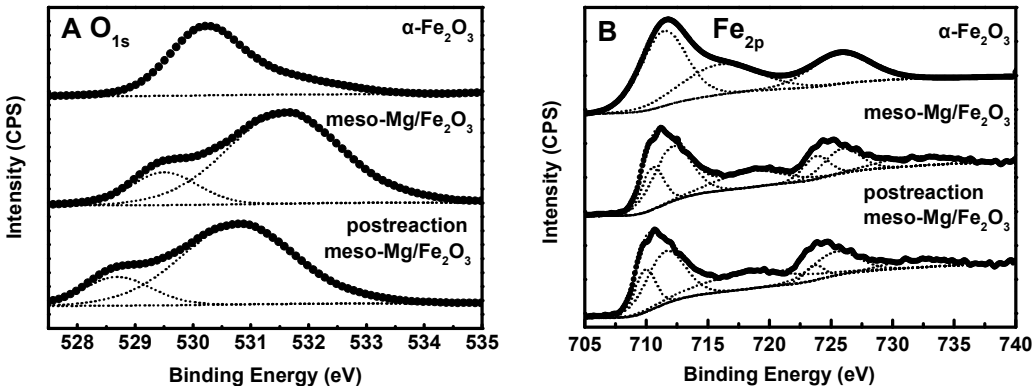

Figure 12. XPS spectra of the α-Fe_2O_3, meso-Mg/Fe_2O_3 and postreaction meso-Mg/Fe_2O_3 samples: O1s (A) and Fe2p (B).

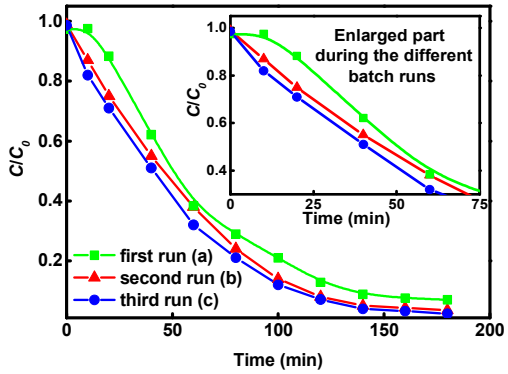

Figure 13. Degradation of methylene blue in different batch runs in the H_2O_2–meso-Mg/Fe_2O_3 system. First run (a), second run (b) and third run (c). (initial pH, H_2O_2 dosage= 2600 $mg \cdot L^{-1}$, initial MB concentration = 60 $mg \cdot L^{-1}$ and catalyst dosage= 0.6 $g \cdot L^{-1}$).

Table 1. The structural and chemical properties of the meso-Mg/Fe_2O_3 and selected iron-based catalysts.

Catalysts	S_{BET} ($m^2 \cdot g^{-1}$)	V_{pore} ($cm^3 \cdot g^{-1}$)	V_{micro} ($cm^3 \cdot g^{-1}$)	D_p (nm)	Mg *wt%*	Fe *wt%*	Mg to Fe Ratio
KIT-6	575	1.08	0.23	6.8	N/A	N/A	N/A
meso-Fe_2O_3	96.3	0.32	0.043	8.6	N/A	76.9	N/A
meso-Mg/Fe_2O_3	90.7	0.37	0.056	9.1	11.0	43.3	0.59
postreaction meso-Mg/Fe_2O_3	190.4	0.44	0.064	12.7	3.67	61.2	0.14
acid washed meso-Fe_2O_3	103.7	0.35	0.049	9.4	N/A	72.3	N/A
acid washed meso-Mg/Fe_2O_3	203.9	0.41	0.061	10.2	3.98	58.7	0.16
con-Mg/Fe_2O_3	9.3	0.06	0.007	-	16.3	68.7	0.54

Fe content in *Wt*%: as determined by ICP-AES analysis; V_{pore}: mesopore volume measured at P/P_0=0.97; V_{micro}: micropore volume calculated from t-plot; D_p: BJH average pore size calculated on the adsorption branch.

Table 2. Effect of pH values on the methylene blue degradation efficiency (%) and iron leaching ($mg \cdot L^{-1}$).

Run No.	pH_0	$[H_2O_2]$ ($mg \cdot L^{-1}$)	Catalyst Dosage ($g \cdot L^{-1}$)	Degradation Efficiency (%)	Fe Leaching ($mg \cdot L^{-1}$)	Mg Leaching ($mg \cdot L^{-1}$)
1	2	2600	0.6	2.3	6.72	-
2	4	2600	0.6	9.5	5.36	-
3	6	2600	0.6	28.2	4.31	-
4	7.5	1600	0.6	91.7	3.17	-
5	7.5	4600	0.6	96.1	4.53	-
6	7.5	2600	0.9	98.7	5.41	-
7	7.5	2600	0.6	93.2	3.45	217.6
First reused meso-Mg/Fe_2O_3	7.5	2600	0.6	96.5	5.13	47.3
Second reused meso-Mg/Fe_2O_3	7.5	2600	0.6	97.8	6.84	36.4

pH_0: initial pH adjusted at the beginning of the degradation of methylene blue, $[H_2O_2]$: initial H_2O_2 dosage, Catalyst Dosage: meso-Mg/Fe_2O_3 used in the reaction, Fe Leaching and Mg Leaching in $mg \cdot L^{-1}$: as determined by ICP-AES analysis.

Table of Contents (TOC) graphic

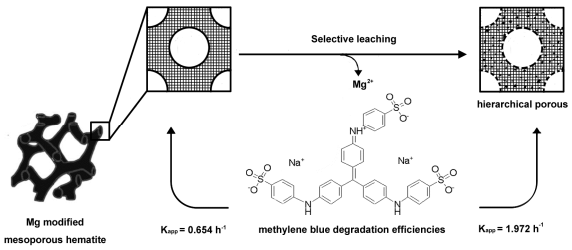

Selective leaching of Mg in Mg modified mesoporous hematite promoted high efficient wet peroxide oxidation of methylene blue.